Consistency of photon emission intensities for efficiency calibration of gamma-ray spectrometers in the energy range from 20 keV to 80 keV

Marie-Christine Lépy, Laurine Brondeau, Yves Ménesguen, Sylvie Pierre, Jonathan Riffaud

CONSISTENCY OF PHOTON EMISSION INTENSITIES FOR EFFICIENCY CALIBRATION OF GAMMA-RAY SPECTROMETERS IN THE ENERGY RANGE FROM 20 KEV TO 80 KEV

Authors: M.-C. Lépy*, L. Brondeau, Y. Ménesguen, S. Pierre, J. Riffaud
Affiliation : CEA, LIST, Laboratoire National Henri Becquerel (LNE-LNHB), Bât.602 PC111, CEA-Saclay 91191 Gif-sur-Yvette Cedex, France

ABSTRACT

The efficiency calibration for different high-purity germanium detectors in the low-energy range was established by the conventional method, using standard radioactive sources. The peak shapes were carefully analysed taking account of natural linewidth, full-energy width at half maximum and scattering. Complementary information was obtained by Monte Carlo simulation using the PENELOPE code, after optimization of the geometrical parameters. This was used to measure photon emission intensities of some low-energy emitting radionuclides, including ^{133}Ba, and compared to the tabulated values.

Keywords: Efficiency calibration, Ba-133, K X-rays, GeHP detector, photon emission intensities

INTRODUCTION

Efficiency calibration of X-ray spectrometers in the low-energy range has been a topic of concern for many years (*e.g.*, Campbell and MacGhee, 1986; Debertin and Helmer, 1988). Two kinds of energy-dispersive detectors are generally used in this energy range, both based on semi-conductor materials (silicon and germanium). Lithium-drifted silicon detectors (Si(Li)), with thickness up to 5 mm, were preferably used in the low-energy range, with the drawback that they require liquid nitrogen cooling. Today, the technology of silicon drift detectors (SDD) makes it possible to benefit from electrical Peltier cooling, but the energy range is still restricted to energies below 50 keV, because of the thinness of the silicon wafer (500 µm). High-purity germanium (HPGe) detectors are very commonly used and planar or semi-planar crystal shapes have been proposed to extend the traditional energy range of coaxial detectors down to 5 keV (Martin and Burns, 1992). Conventional efficiency calibration of the spectrometers relies on experimental measurement of standard radionuclides. Complementary approaches based on Monte Carlo simulation have also been developed (see *e.g.* Helmer *et al.* (2003), Peyres and García-Toraño (2007), Sima and Arnold (2009)). Maidana *et al.* (2013) performed a mixed study utilizing an analytical expression as proposed by Seltzer (1981) which takes into account the different interactions in the detector. Plagnard *et al*. (2007) used a tunable monochromatic X-ray source and a reference proportional counter in an innovative experiment to calibrate the intrinsic efficiency of an HPGe detector, without any radioactive source. Any alternative approach nevertheless requires validation with standard sources to check the consistency of calculation with experiment and/or to determine the effective detection solid angle. Barium-133 and americium-241 are frequently used in the low-energy range, where only a few gamma-emitting radionuclides are available for this purpose. But we observed systematic deviations, with relative differences of about 2-3%, between the full-energy peak (FEP) efficiencies experimentally obtained for the peaks at 53 keV (^{133}Ba) and 59.6 keV (^{241}Am), despite the small energy gap between them. It was then decided to collect further information and to examine in detail the experimental FEP

calibration in the low-energy range for HPGe detectors with different sizes to improve the consistency of the photon emission intensities in the 20-80 keV energy region.

EXPERIMENTAL CONDITIONS

At the Laboratoire National Henri Becquerel (LNHB), X-ray spectrometry is performed with N-type HPGe detectors. Four detectors are available for the present study and their main characteristics are reported in Table 1. Each spectrometer is calibrated with standard point sources installed at the reference distance. For each energy, E, the full-energy peak (FEP) efficiency, $\varepsilon(E)$, is derived from the net counting, N(E) according to:

$$\varepsilon(E) = \frac{N(E)}{A \cdot I(E) \cdot t} \prod_i C_i \qquad \text{(Eq. 1)}$$

where:

A is the activity of the standard radionuclide (Bq),

I(E) is the emission intensity of the line with energy *E*,

t is the acquisition duration (live time) (seconds),

C_i stands for different correction factors (radioactive decay, coincidence summing, etc.).

The standard sources are prepared at LNHB from radioactive solutions calibrated by primary methods, thus their activity is characterized with standard relative uncertainty of 0.5% or less. For the practical use, to derive the efficiency for any energy, the set of raw data (energies and efficiencies) is fitted using a log-log polynomial function, taking into account the correlations between input data. An example of the experimental data and the resulting calibration curve in the range from 12 keV to 120 keV for detector G1 is plotted in Figure 1. Relative standard combined uncertainties are about 1 % to 2 % in the energy range of interest. The fitted calibration curves versus the energy for the four detectors are compared in Figure 2. Whereas, the efficiency of the two coaxial detectors decreases strongly in the low-energy part, it keeps a rather stable value in the range from 40 keV to 60 keV. On the other hand, the efficiency of the smaller detector is quite constant between 20 keV and 40 keV

and then decreases due to its small active thickness. The present study focusses on two topics: 1) The ^{133}Ba absolute gamma-ray intensities based on data recorded with the two large coaxial detectors (G1 and G2) and experimental efficiency calibration; and 2) the KX-ray emission intensity ratios of selected nuclides based on the information derived from measurements and Monte Carlo simulations with the smaller detectors (G3 and G4).

PEAK PROCESSING

The net areas of the full-energy peaks were obtained with the COLEGRAM software (Ruellan *et al.*, 1996), which proposes different mathematical functions to fit the experimental points by the least-squares minimization method, and paying particular attention to the following:

1. Natural linewidth of the incident photons;
2. Full-width at half maximum versus energy;
3. Scattering effects.

As discussed early by Debertin and Pessara (1981), one has to distinguish between peaks shapes resulting from interactions of X-rays and the ones induced by gamma-rays. The observed peak width results from the convolution of the so-called natural line width, due to the intrinsic nature of the incident photons, by the Gaussian broadening induced by the charge pair creation statistics. The energy distribution of a gamma emission, due to transitions between nuclear levels is well defined and has a Lorentzian shape whose width is a few meV. The X-ray emission is linked to atomic relaxation and the intrinsic Lorentzian width ranges from some eV to some tens of eV, depending on the atomic number of the element, Z, and on the electronic (sub)-shells concerned in the atomic rearrangement. Consequently, according to the energy range and the detector energy resolution, the X-ray linewidth cannot always be considered as negligible and must be taken into account in the fitting procedure used. Thus a Voigt function (convolution of a Lorentzian function by a Gaussian shape) is used:

$$V(E) = \int_{-\infty}^{+\infty} L(E') \cdot G(E - E') \cdot dE' \qquad \text{(Eq. 2)}$$

where:

$$G(E) = \frac{A}{\sigma\sqrt{2\pi}} \exp\left(\frac{-(E - E_0)^2}{2\sigma^2}\right) \qquad \text{(Eq. 3)}$$

$$L(E) = \frac{\Gamma/2\pi}{(E - E_0)^2 + (\Gamma/2)^2} \qquad \text{(Eq. 4)}$$

The standard deviation of the Gaussian, σ, and the Lorentzian width, Γ, are quoted in Table 2 for some typical energies and detectors G2 and G4. The ratio σ/ Γ is about 30 for the large detector (G2) and the Gaussian shape dominates in this case, but it is only about 8 for the small detector (G4) and consequently it is necessary to use the Voigt shape to fit the experimental peaks recorded with this one. The natural linewidths are taken from tabulated data (Campbell and Papp, 2001) and kept constant in the fitting procedure, although the associated relative uncertainties are estimated to be around 10 % at the minimum. A typical example of the fitting of X-rays using either a pure Gaussian or a Voigt shape is presented in Figure 3. The spectrum obtained with detector G4 shows the Kβ peaks of cesium emitted in the decay of ^{133}Ba. The improvement of the fitting procedure is clearly seen in the lower parts of the peaks. The relative differences for the areas derived from the two processes are respectively 1.8% and 2.2% for the 35.15 keV and 36.01 keV energies.

It is generally accepted that the full-width at half maximum (FWHM) of a FEP includes two main contributions: a constant part mainly due to electronic noise and an energy-dependent component resulting from the statistical scattering of the number of charge carriers created in the bulk of the semiconductor. The statistical variation of the number of electron-hole pairs depends on the incident energy, *E*, on the Fano factor of the semiconductor material (Fano, 1947), *F*, and on the mean pair creation energy, *w*. The standard deviation of the Gaussian representing the main part of the each peak, can then be expressed as a function of the energy, *E*:

$$\sigma^2(E) = \sigma_0^2 + F \cdot w \cdot E \qquad \text{(Eq. 5)}$$

It is checked that the square of the Gaussian standard deviation follows a linear variation versus the incident energy (Figure 4). In the present case, the slope of the fitted linear function is 0.307; assuming that the mean energy for creating an electron-hole pair in germanium at 77K is w= 2.97 eV, this gives a value of 0.103 for the Fano factor of this detector G4. The Gaussian standard deviation value is important information which is directly linked to the resulting peak area. In the case of very close overlapping peaks -*e.g.*, the L X-rays of neptunium in the decay of ^{241}Am- this means that the standard deviation value can be imposed to get the individual peak areas.

A further effect has to be examined in low-energy spectra since scattering causes low-energy tailing close to the FEPs of interest. It strongly depends on the geometrical conditions and increases with the amount of materials (including air) around the source-detector arrangement. As an example, Figure 5 shows the spectrum measured with detector G2 for a source of ^{129}I, which decays by beta minus decay to an excited level at 39.58 keV in ^{129}Xe. The gamma transition is highly converted, thus intense K X-rays of xenon with energies 29.67 keV (Kα) and 33.83 keV (Kβ) are emitted together with the 39.58-keV gamma–ray. The three corresponding peaks are accompanied by a bump on the left side, whose relative position and intensity depend both on the energy, as discussed by Plagnard *et al.* (2008). To keep the same approach on the whole energy range, it was chosen to fit the peaks only with Gaussian shapes (or Voigt shapes for the X-rays), without including any tailing. It is assumed that the weight of high content channels is large enough to allow unambiguous fitting of the Gaussian width and the associated contribution in the lower part of the peak. Thus, the calculated peak areas represent only the interactions of emitted photons that did not suffer any scattering, whatever the source shape.

MONTE CARLO SIMULATION

For the smaller detector (G4), the experimental approach was completed by performing Monte Carlo simulation with the PENELOPE code (Salvat *et al.*, 2015). The FEP efficiency is obtained as the ratio of the number of events corresponding to the release of all the incident energy in the detector, divided

by the number of simulated particles (photons with energy *E*): This corresponds to the Gaussian part of the experimental FEPs. The detection geometry was modelled according to the supplier specifications, including additional geometrical details obtained from a radiograph and from a previous experiment in which the dimensions of the internal collimator and absorbing materials were carefully measured (Plagnard *et al.*, 2007). The dimensions were optimized by comparison with the experimental results. The entrance dead layer thickness had to be increased from 0.01 µm to 0.7 µm to fit the efficiency in the low-energy region. For the energy range above 40 keV, the model could not reproduce the experimental results. In spite of dramatically reducing the active layer (increase of the bottom dead layer) the simulation produced results significantly higher than the experiment. The hypothesis of a dysfunction of the digital electronic module for processing signals in the high energy range (saturation due to large amplitude signals) could explain such a result.

RESULTS AND DISCUSSION

Gamma emission intensities of Ba-133

The fitted efficiency curves of detectors G1 and G2, without including data from ^{133}Ba, are used to calculate the gamma emission intensities, *I(E)*, of ^{133}Ba by inversion of Eq.1. It must be noted that measurements were performed using different barium sources, but from a homogeneous set prepared with the same reference mass activity (with a relative combined uncertainty of 0.43%), so the final result is the mean value, with the uncertainty associated to one measurement. These are compared to the evaluated data (Reference DDEP) in Table 3, where the intensities of peaks with energies higher than 120 keV are also presented. The main differences are noted for the lines with energies 53.16 keV, 81.00 keV and 223.24 keV. Both the 53.16 keV and 223.24 keV peaks are superimposed on a rather flat background and the area determination presents no difficulty since they are well isolated. The 79.61-81.00 keV doublet could also be easily processed and the individual area of each peak accurately determined, especially with the smaller detector (G4) as shown in Figure 6. Consequently, the combined standard uncertainty associated to the 79.61 keV emission is significantly reduced compared to the tabulated value.

K X-ray emission intensities

The absolute X-ray emission intensities are preferably derived from measurements performed with the detector G4, thanks to its superior energy resolution in the energy range where its detection efficiency remains stable. The experimental results obtained for 6 radionuclides which can be used for efficiency calibration in the low-energy range (^{85}Sr, ^{88}Y, ^{109}Cd, ^{133}Ba, ^{152}Eu and ^{166m}Ho) are presented in Table 4 and compared with evaluated data. There is a tendency to obtain Kβ/Kα experimental ratios slightly lower than the tabulated ones for the first two elements, while they are higher for the last four elements; however, both series of data agree within the uncertainties. The absolute emission intensities of Kα X-rays are detailed in Table 5, together with the evaluated data. The present measured ratios Kα2/Kα1 are in close agreement with the tabulated ones.

CONCLUSION

In this study, the absolute photon emission intensities of Ba-133 and the absolute X-ray emission intensities in the decays of ^{85}Sr, ^{109}Cd, ^{133}Ba, ^{152}Eu and ^{166m}Ho were determined using HPGe detectors. These results are obtained with combined standard uncertainty of 2 % at maximum. They are compared with the evaluated values and most of them agree, however, small differences are noticed for 3 gamma lines of Ba-133. It must be noted that in the evaluation procedure (DDEP, 2017), the X-ray emission intensities are derived from the fluorescence yields and relative Kβ/Kα intensities obtained from the compilation of Schönfeld and Janssen (1996), while theoretical calculations of Scofield (1974) are used to compute the partial ratios Kα2/Kα1. Since there is a strong correlation between the selected atomic data, this is also the case for the tabulated X-ray emission intensities. Consequently, the experimental efficiency calibration obtained with radionuclides is also directly affected by this correlation. According to Campbell (2010) in a review of the present knowledge of X-ray atomic parameters, it is always of interest to provide additional measurements of photon emission intensities.

REFERENCES

Campbell, J.L., McGhee, M.C., 1986. *State-of-the-art efficiency determination for a Si(Li) X-ray detector in the 3-40 keV energy range.* Nuclear Instruments and Methods in Physics Research A248, 393-404.

Campbell, J.L., Papp,T., 2001. *Widths of the atomic K-N7 levels*. Atomic Data and Nuclear Data Tables 77, 1–56.

Campbell, J.L., 2010. *X-Ray Energies: Transition Probabilities, Fluorescence and Coster-Kronig Probabilities*. International Radiation Physics Society Bulletin 24 (1), 17-30.

DDEP, 2017, http://www.nucleide.org/DDEP_WG/Introduction_2011.pdf

Debertin, K., Helmer, R.G., 1988. *Gamma- and X-ray spectrometry with semiconductor detectors.* Ed. North Holland.

Debertin, K., Pessara, W., 1981. *Natural line-width effects in gamma- and X-ray emission rate measurements with semiconductor detectors*. Nuclear Instruments and Methods 184 (2–3), 497-503.

Fano, U., 1947. *Ionization yield of radiations II. The fluctuations of the number of ions*. Physical Review 72, 26-29.

Helmer, R.G., Hardy, J.C., Iacob, V.E., Sanchez-Vega, M., Neilson, R.G., Nelson, J., 2003. *The use of Monte Carlo calculations in the determination of a Ge detector efficiency curve*. Nuclear Instruments and Methods in Physics Research A511, 360-381.

Lépy, M.-C., Plagnard, J., Ferreux, L., 2008. *Determination of ^{241}Am L X-ray emission intensities.* Applied Radiation and Isotopes 66, 715-721.

Maidana, N. L., Vanin, V. R., Jahnke, V., Fernández-Varea, J.-M., Martins, M. N., Brualla L., 2013. *Efficiency calibration of x-ray HPGe detectors for photons with energies above the Ge K binding energy*. Nuclear Instruments and Methods in Physics Research A729, 371–380.

Martin, L. J., Burns, P. A., 1992. *The HPGe as a defined-solid-angle detector for low-energy photons*, Nuclear Instruments and Methods in Physics Research A312, 146–151.

Peyres, V., García-Toraño, E., 2007. *Efficiency calibration of an extended-range Ge detector by a detailed Monte Carlo simulation.* Nuclear Instruments and Methods in Physics Research A 580, 296-298.

Plagnard, J., Bobin, C., Lépy, M.-C., 2007. *Accurate efficiency calibration of a low-energy HPGe detector using a monochromatic X-ray source*. X-ray Spectrometry 36, 191–198.

Plagnard, J., Hamon, C., Lépy, M.-C., 2008. *Study of scattering effects in gamma-ray spectrometry*. Applied Radiation and Isotopes 66, 769-773.

Ruellan H., Lépy, M.-C., Etcheverry, M., Plagnard, J., Morel, J., 1996. *A new spectra processing code applied to the analysis of ^{235}U and ^{238}U in the 60 to 200 keV energy range.* Nuclear Instruments and Methods in Physics Research A369, 651-656.

Salvat F., Fernandez-Varea, J.-M., Sempau, J.,2015. *PENELOPE-2014: A Code System for Monte Carlo Simulation of Electron and Photon Transport*. OECD

Schönfeld, E., Janßen, H., 1996. *Evaluation of atomic shell data*. Nuclear Instruments and Methods in Physics Research A369, 527-533.

Scofield, J.H., 1974. *Relativistic Hartree Slater values for K and L X-ray emission rates*. Atomic Data and Nuclear Data Tables 14, 121-137.

Seltzer, S. M., 1981. *Calculated response of intrinsic Germanium detectors to narrow beams of photons with energies up to ∼300 keV*. Nuclear Instruments and Methods 188, 133–151.

Sima, O., Arnold, D., 2009. *On the Monte Carlo simulation of HPGe gamma-spectrometry systems*. Applied Radiation and Isotopes 67, 701-705.

Table 1: Main characteristics of the HPGe detectors

HPGe detector	G1	G2	G3	G4
Crystal geometry	Coaxial	Coaxial	Planar	Planar
Crystal diameter	49.5 mm	48.7 mm	15.1 mm	2 mm
Crystal thickness	47.8 mm	55.4 mm	6.7 mm	1 mm
Dead layer thickness	0.3 µm	0.3 µm	0.8 µm	0.7 µm
Beryllium window thickness	500 µm	500 µm	127 µm	10 µm
Energy resolution (Full Width at Half Maximum at 5,9 keV)	-	-	225 eV	140 eV
Energy resolution (Full Width at Half Maximum at 59 keV)	670 eV	690 eV	370 eV	330 eV
Calibration distance (source-to-detector window)	10.7 cm	10.3 cm	7.8 cm	3.7 cm (In vacuum)

Table 2: Comparison of Lorentzian and Gaussian widths for some photon energies

(The Lorentzian widths are fixed and the relative uncertainties on the Gaussian standard deviations are a few 10-3.)

Energy (keV)	Type of emitted photon	Natural Lorentzian width (eV)	Fitted Gaussian standard deviation* (σ) (eV)	
			G2	G4
14.4	^{57}Co - gamma ray	Negligible	275	71.8
17.5	^{241}Am – XLβ1	11.6	293	93.8
22.1	^{109}Cd – Ag XKα	8.91	302	90.6
21	^{241}Am – XLγ1	13.9	304	95.2
26.4	^{241}Am - gamma ray	Negligible	276	97.5
30.6	^{133}Ba - Cs XKα1	15.5	270	106
40.1	^{152}Eu – Sm XKα1	13.5	309	119
45.4	^{152}Eu – Sm XK β1	27.9	314	139
53.1	^{133}Ba - gamma ray	Negligible	291	134
59.6	^{241}Am -gamma ray	Negligible	292	141

Energy	Gamma emission intensities (per 100 decays)		
(keV)	**DDEP 2004**	**This work**	**DDEP 2016**
53.16	2.14 (3)	2.229 (23)	2.14 (6)
79.61	2.65 (5)	2.633 (27)	2.63 (19)
81.00	32.9 (3)	34.08 (33)	33.31 (30)
160.61	0.638 (4)	0.634 (7)	0.638 (6)
223.24	0.453 (3)	0.459 (5)	0.450 (5)
276.40	7.16 (5)	7.22 (6)	7.13 (6)
302.85	18.34 (13)	18.42 (14)	18.31 (11)
356.01	62.05 (19)	62.45 (45)	62.05 (19)
383.85	8.94 (6)	8.94 (7)	8.94 (6)

Table 3 : Result of the measurement of gamma emission intensities in the decay of ^{133}Ba compared with evaluated data (DDEP)

	This work			NUCLEIDE		
Radionuclide	XKalpha	XKbeta	Kβ/Kα (%)	I Kalpha	I Kbeta	Kβ/Kα (%)
^{85}Sr (Rb XK)	48.4 (16)	8.35 (30)	0.173 (8)	50.20 (33)	8.97 (11)	0.179 (2)
^{88}Y (Sr XK)	53.4 (9)	9.52 (19)	0.178 (5)	51.26 (31)	9.4 (11)	0.183 (2)
^{109}Cd (Ag XK)	85.8 (16)	18.46 (34)	0.215 (6)	84.31 (58)	17.90 (22)	0.212 (3)
^{133}Ba (Cs XK)	94.7 (16)	22.66 (40)	0.239 (6)	96.2 (8)	22.69 (31)	0.236 (4)
^{137}Cs (Ba XK)	5.51 (9)	1.317 (22)	0.239 (6)	5.54 (8)	1.321 (23)	0.238 (5)
^{152}Eu (Sm)	57.2 (10)	14.27 (25)	0.249 (6)	58.5 (6)	14.82 (21)	0.253 (4)
^{152}Eu (Gd)	0.676 (14)	0.178 (5)	0.263 (9)	0.680 (14)	0.174 (4)	0.256 (8)
^{166m}Ho (XK Er)	28.6 (6)	7.87 (37)	0.275 (14)	30.01 (45)	7.86 (15)	0.262 (6)

Table 4: Result of the measurement of K X-ray emission intensities (per 100 decays) of some radionuclides compared with evaluated data (DDEP, 2017)

	This work		NUCLEIDE	
	X-ray emission intensity per 100 decays	Kα2/Kα1	X-ray emission intensity per 100 decays	Kα2/Kα1
^{109}Cd (Ag Kα2)	29.9 (6)	0.534 (14)	29.21(30)	0.530 (7)
^{109}Cd (Ag Kαl)	55.9 (10)		55.1(50)	
^{133}Ba (Cs Kα2)	33.4 (6)	0.545 (14)	33.8(4)	0.542 (8)
^{133}Ba (Cs Kα1)	61.3 (11)		62.4(7)	
^{152}Eu(Sm Kα2)	20.43 (35)	0.555 (13)	20.8(3)	0.552 (11)
^{152}Eu(Sm Kα1)	36.8 (6)		37.7(5)	
^{152}Eu(Gd Kα2)	0.238 (5)	0.542 (18)	0.243(7)	0.556 (22)
^{152}Eu(Gd Kα1)	0.439 (11)		0.437(12)	
^{166m}Ho(Ek Kα2)	10.36 (19)	0.566 (15)	10.81(21)	0.563 (16)
^{166m}Ho(Ek Kα1)	18.29 (33)		19.2(4)	

Table 5 : Detail of the emission intensities of Kalpha X-rays of some radionuclides compared with evaluated data (DDEP, 2017)

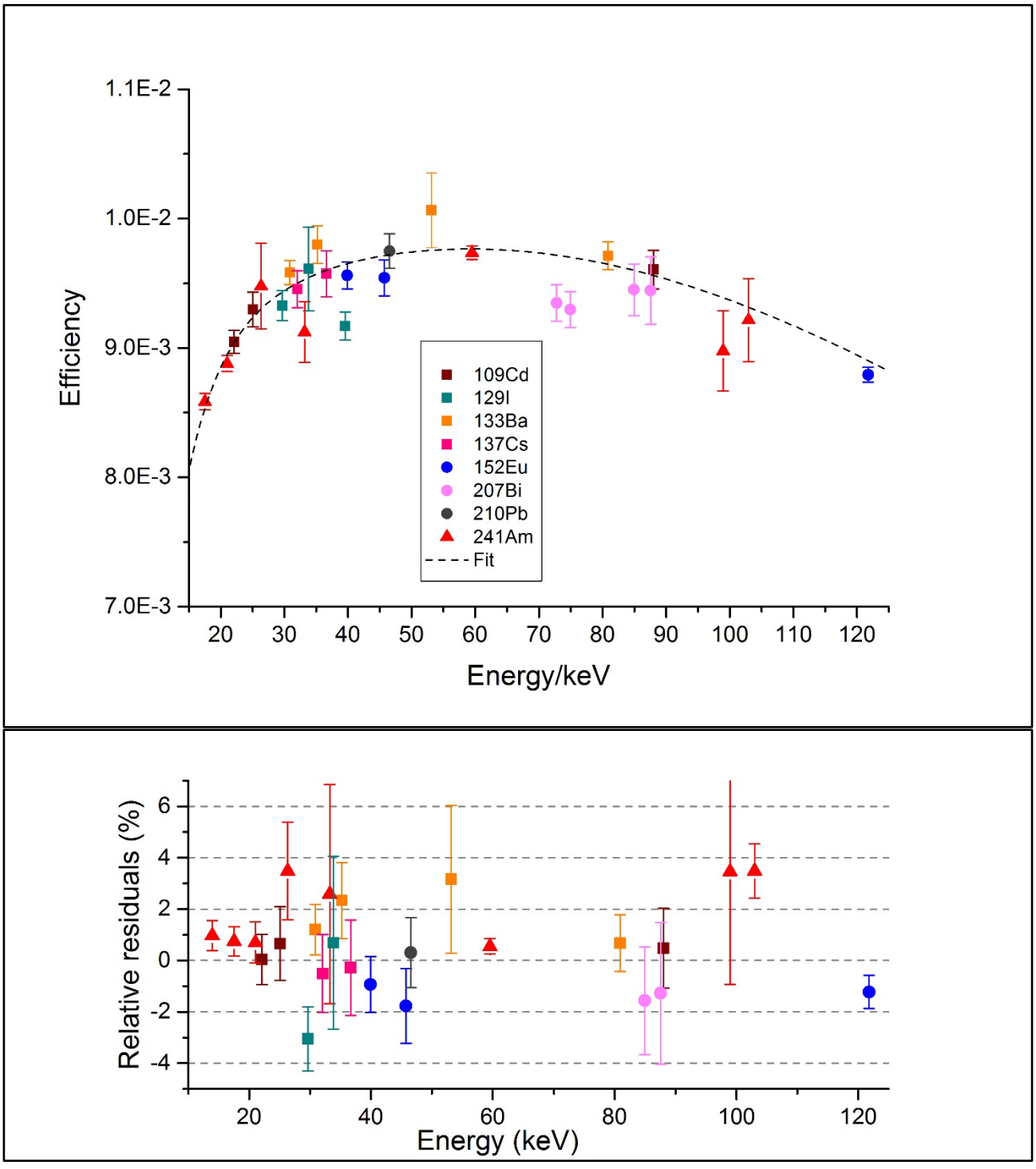

Figure 1: Efficiency calibration of detector G1 for point sources – Experimental values and fitted curve. The relative residuals are plotted in the lower panel

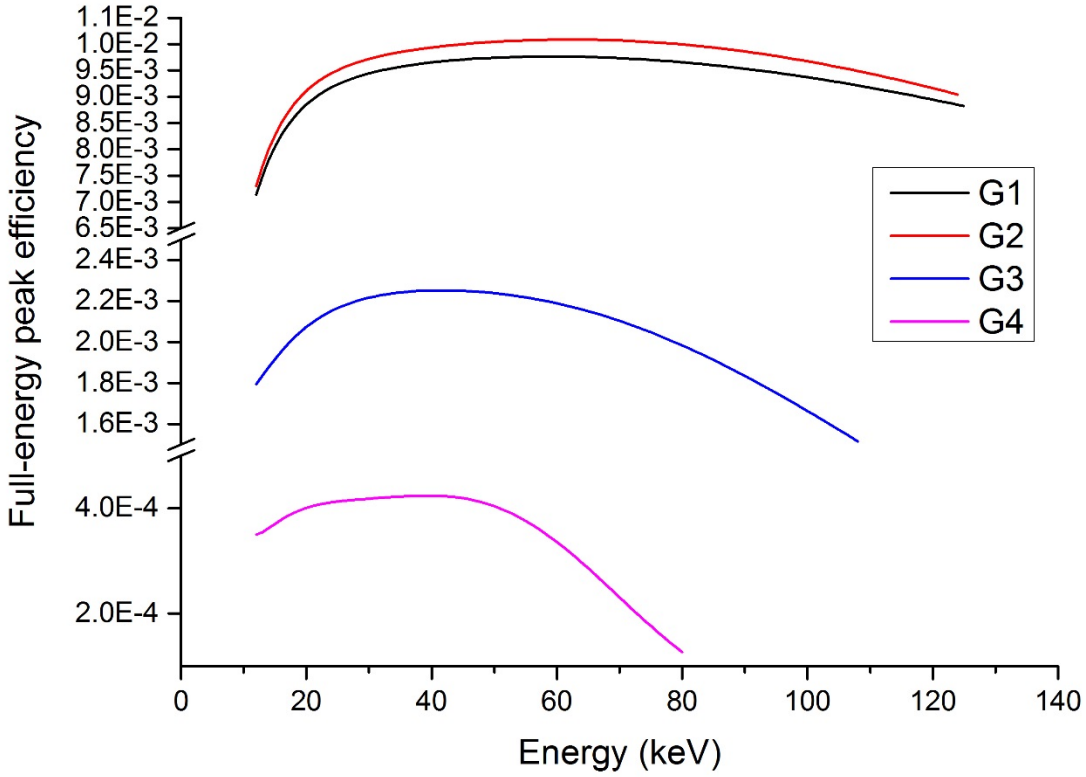

Figure 2: Comparison of the efficiency calibration for the 4 HPGe detectors for point sources.

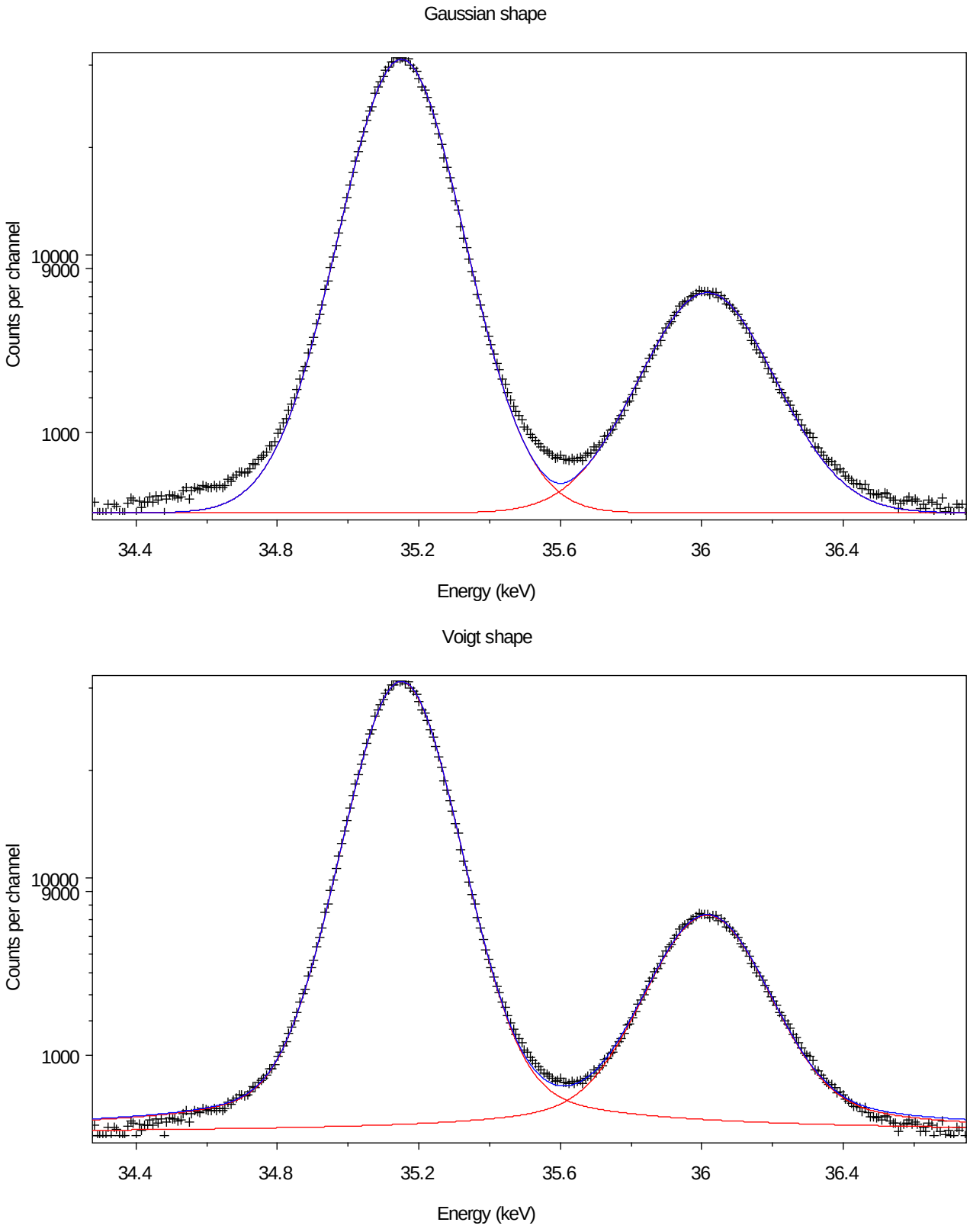

Figure 3 : Example of fitting of K X-rays of ^{133}Ba (K beta region) for detector G4 – Using Gaussian function (upper panel) and using Voigt function (lower panel).

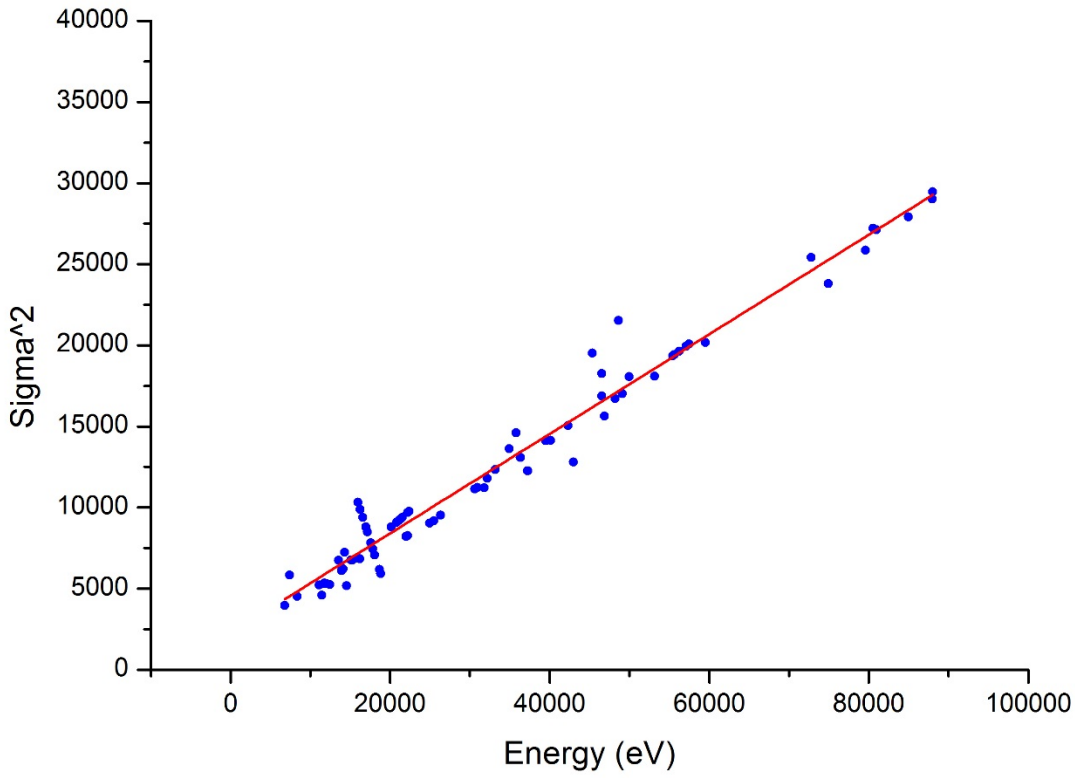

Figure 4 : Evolution of the square of the Gaussian standard deviation versus the energy (Detector G4)

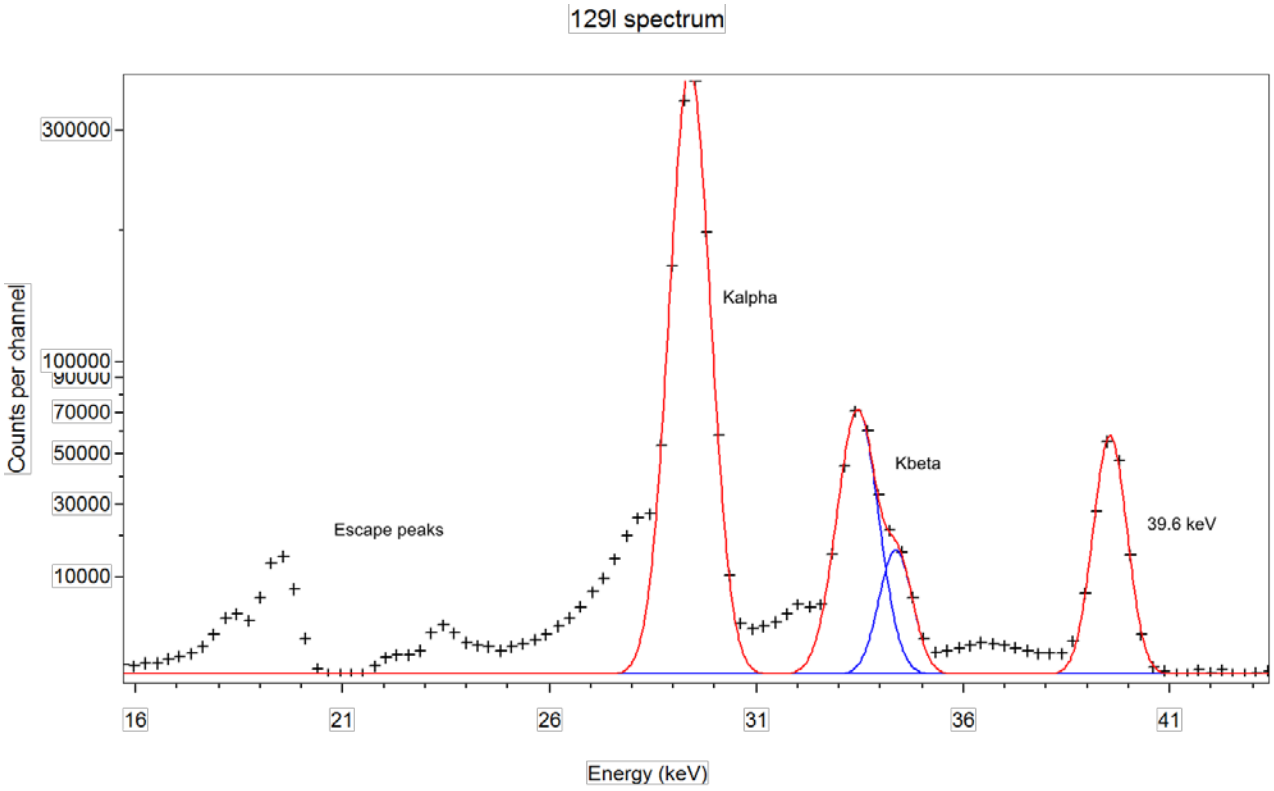

Figure 5 : Spectrum of ^{129}I, with full-energy peaks at 29.67 keV, 33.83 keV (XK) and 39.58 keV (Gamma) and respective tailings due to scattering (Detector G2)

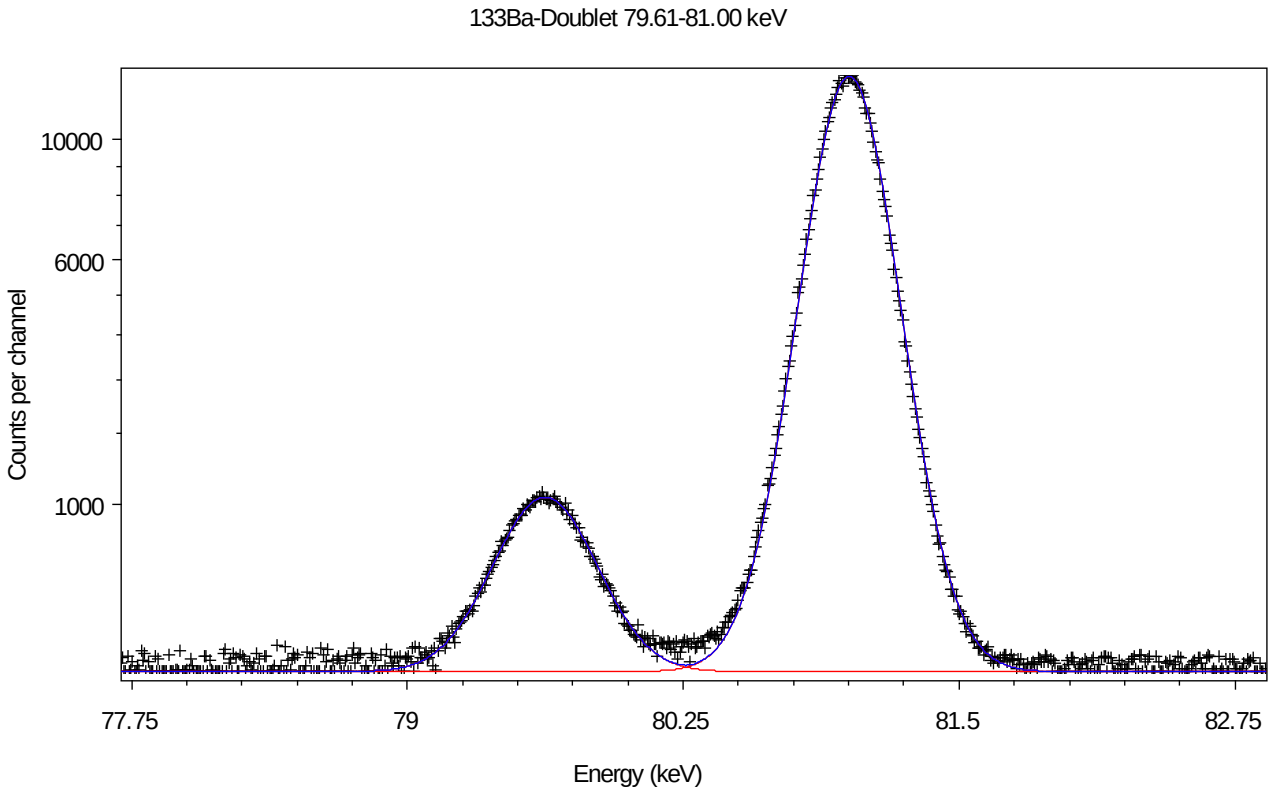

Figure 6 : Deconvolution of the 79.61-81.00 keV doublet of ^{133}Ba (Detector G4)